Journal of
Materials Chemistry A

Accepted Manuscript

This article can be cited before page numbers have been issued, to do this please use: S. Huang, G. Zhang, N. S. Knutson, M. T. Fontana, R. C. Huber, A. S. Ferreira, S. Tolbert, B. J. Schwartz and Y. Rubin, *J. Mater. Chem. A*, 2015, DOI: 10.1039/C5TA07688A.

ROYAL SOCIETY OF CHEMISTRY

www.rsc.org/materialsA

DOI: 10.1039/C5TA07688A

Journal of Materials Chemistry A

ARTICLE

Beyond PCBM: Methoxylated 1,4-Bisbenzyl [60]Fullerene Adducts for Efficient Organic Solar Cells

Received 00th January 20xx,
Accepted 00th January 20xx

DOI: 10.1039/x0xx00000x

www.rsc.org/

Shaohua Huang, ‡[a] Guangye Zhang,‡[a] Nicholas S. Knutson,[a] Matthew T. Fontana,[a] Rachel C. Huber,[a] Amy S. Ferreira,[a] Sarah H. Tolbert,*[ab] Benjamin J. Schwartz*[a] and Yves Rubin*[a]

Organic solar cells have been based mostly on conjugated polymers and the classic fullerene derivative PCBM and are characterized by modest open circuit voltages (V_{oc}). Increasing V_{oc} requires fullerene acceptors with higher LUMOs than PCBM. To date, most fullerene derivatives synthesized for this purpose either do not achieve the high photocurrent afforded by PCBM or show relatively poor compatibility with the next-generation low bandgap conjugated polymers used in high-efficiency organic solar cells. Here, we report the facile synthesis of methoxylated 1,4-bisbenzyl fullerene adducts and their application as efficient electron acceptors in conjugated polymer-based solar cells. The methoxy groups are found to be essential to increasing the LUMO levels, and accordingly the V_{oc}, of the devices compared to the parent 1,4-bisbenzyl fullerene, and more importantly, to PCBM. The best fullerene 1,4-bisadduct provides a ~20% enhancement in power conversion efficiency over PCBM when used with the classic crystalline polymer P3HT. When used in combination with a higher-performance low bandgap polymer, PTB7, the bisadduct both increases the device open-circuit voltage and maintains the high photocurrent provided by the more traditional PCBM. We also examine 10 different 1,4-fullerene bisadducts and show that the photovoltaic device performance is strongly influenced by the number and relative position of the methoxy substituents on the benzyl addends: moving a single methoxy substituent by one position on the benzyl rings can change the device efficiency by over a factor of 2.

Introduction

Organic solar cells have received great attention in recent years as a potential alternative to silicon solar cells because of their ability to be inexpensively solution-processed and because they can be lightweight and flexible.[1–5] The key component of an organic-based photovoltaic system is its active layer, wherein a *p*-type conjugated polymer and an *n*-type acceptor material mix to form a bicontinuous interpenetrating network that is referred to as a bulk heterojunction (BHJ).[6,7] Fullerene derivatives have been used extensively as the acceptors in BHJ solar cells thanks to their high electron affinities and electron mobilities.[8] The power conversion efficiency (PCE) of polymer/fullerene BHJ solar cells can be as high as 10.8%,[9] with most of the recent advances coming from the design of new polymer donors and/or the use of new device architectures.[10,11] In contrast, progress on the design and synthesis of novel fullerene acceptors for high-efficiency organic photovoltaics has been much less rapid. Most of the highest performing devices[9,12] still utilize the classic fullerene derivative [6,6]-phenyl-C-61-butyric acid methyl ester (PCBM), synthesized more than twenty years ago,[13] or its expensive C_{70} analogue, $PC_{71}BM$.[14]

The PCE of a solar cell is proportional to the product of the short-circuit current (J_{sc}), open-circuit voltage (V_{oc}) and fill factor (*FF*). Thus, one strategy for improving device efficiency is to increase the V_{oc}, which is directly related to the difference between the energy of the highest occupied molecular orbital (HOMO) of the polymer donor and that of the lowest unoccupied molecular orbital (LUMO) of the fullerene acceptor. As long as the LUMO of the fullerene is lower than that of the polymer by an amount sufficient to promote charge separation, raising the fullerene LUMO level should increase the V_{oc} and thus the PCE.

To this end, several research groups have synthesized fullerene derivatives where two or more double bonds of the fullerene cage are saturated.[15–24] Although V_{oc} has been demonstrated to increase with this method, devices based on most of these new fullerenes fail to maintain high J_{sc} and/or *FF*, and as a result, the overall device efficiency suffers.[19,25–27] This is because altering the chemical structure of a fullerene addend can have detrimental effects on device performance for two reasons: first, the size and pattern of the addends can

[a] Department of Chemistry and Biochemistry, University of California, Los Angeles, 607 Charles E. Young Drive East, Los Angeles, California 90095-1569, United States. E-mail: schwartz@chem.ucla.edu, rubin@chem.ucla.edu
[b] Department of Materials Science and Engineering, University of California, Los Angeles, Los Angeles, California 90095-1569, United States. tolbert@chem.ucla.edu

†Electronic Supplementary Information (ESI) available: Details of synthesis of fullerene derivatives **1a–1k**, NMR spectra, mass spectrometry data, device fabrication procedures for photovoltaic devices, table of ideality factors, series resistance and shunt resistance for all photovoltaic devices, details of UV-visible absorption and 2-D GIWAXS measurements, the measured external quantum efficiency, cyclic voltammetry measurements and the summary of fullerene LUMO levels. See DOI: 10.1039/x0xx00000x

‡These authors contributed equally to this work. The authors declare no competing financial interest.

View Article Online
DOI: 10.1039/C5TA07688A

dramatically influence the electronic coupling between adjacent fullerenes through steric and/or electronic effects, causing a significant decrease in local electron mobility;[27] and second, changes in the fullerene addends can alter the degree of phase separation from the polymer, sometimes caused by a reduction in fullerene crystallinity due to packing constraints or mixtures of isomers. In cases where fullerene crystallization drives phase separation, this can dramatically change the morphology of the bulk heterojunction.[27]

There are a few select fullerene derivatives, such as the bisadduct of PCBM (*bis*-PCBM)[28], indene C_{60} bisadduct (ICBA)[15] and its C_{70} congeners,[29] dihydronaphthyl-based C_{60} bisadduct (NCBA)[30] and di(4-methyl-phenyl)methano-C_{60} bisadduct (DMPCBA),[31] that have shown good photovoltaic performance when used in combination with the classic crystalline semiconducting polymer poly(3-hexylthiophene-2,5-diyl) (P3HT). However, when these fullerene derivatives are used in combination with less crystalline state-of-the-art low-bandgap polymers, the performance of the solar cells is typically low, with greatly decreased J_{sc} and *FF*.[25,26,32–34] Therefore, despite the aforementioned efforts to increase the V_{oc}, PCBM (and its C_{70} analogue) are still the most successful fullerene acceptors for high-performance polymer-based photovoltaics to date.

In order to design new fullerene acceptors for high performance polymer-based solar cells, the following factors need to be considered: 1) The LUMO level of the fullerene derivative should be carefully tuned so that when paired with the polymer of choice, an ideal energy level offset between the fullerene donor and polymer acceptor is attained. Although still under debate,[34,35] the generally accepted range of this offset is about 0.3 eV, depending on the materials.[26,36,37] 2) Size-suitable addends are needed to assist close contacts between fullerene balls, thereby facilitating favorable electronic coupling to facilitate charge transport within the fullerene domains.[27,38] 3) Derivatives must possess good solubility in organic solvents for solution processing, and must form reasonable BHJ structures with a variety of polymers. In this paper, we thus present the synthesis of a series of new fullerene derivatives that satisfy all of these requirements. We find that when carefully designed, fullerenes with higher LUMOs can be prepared that produce devices with higher V_{oc}'s – without significant loss of J_{sc} or *FF* – and thus higher power conversion efficiencies.

Our new derivatives are methoxylated 1,4-bisbenzyl fullerene adducts (MeO-BBF, Table 1), i.e. two addends are located at the "*para*" positions of a six-membered ring on the fullerene cage.[39] These derivatives have a smaller π-conjugated system with reduced symmetry[40–43] resulting in a slightly higher LUMO level than the corresponding 1,2-fullerene bisadducts. The LUMO level, side chain nature and solubility of the 1,4-fullerene bisadducts can be further tuned by altering each addend independently.[39] The molecules we focus on bear electron-donating methoxy group(s) on the benzyl ring(s). Since these electron-rich methoxy substituents are not conjugated with the fullerene π-system, they would be expected to have negligible electronic interaction. However, we find through experiments that are supported by DFT calculations that the relative position and number of methoxy groups can have a dramatic effect on the performance of these fullerene derivatives in polymer-based solar cells.

Table 1 Synthesis of symmetric and asymmetric 1,4-bisbenzyl fullerene C_{60} adducts **1a–k**.

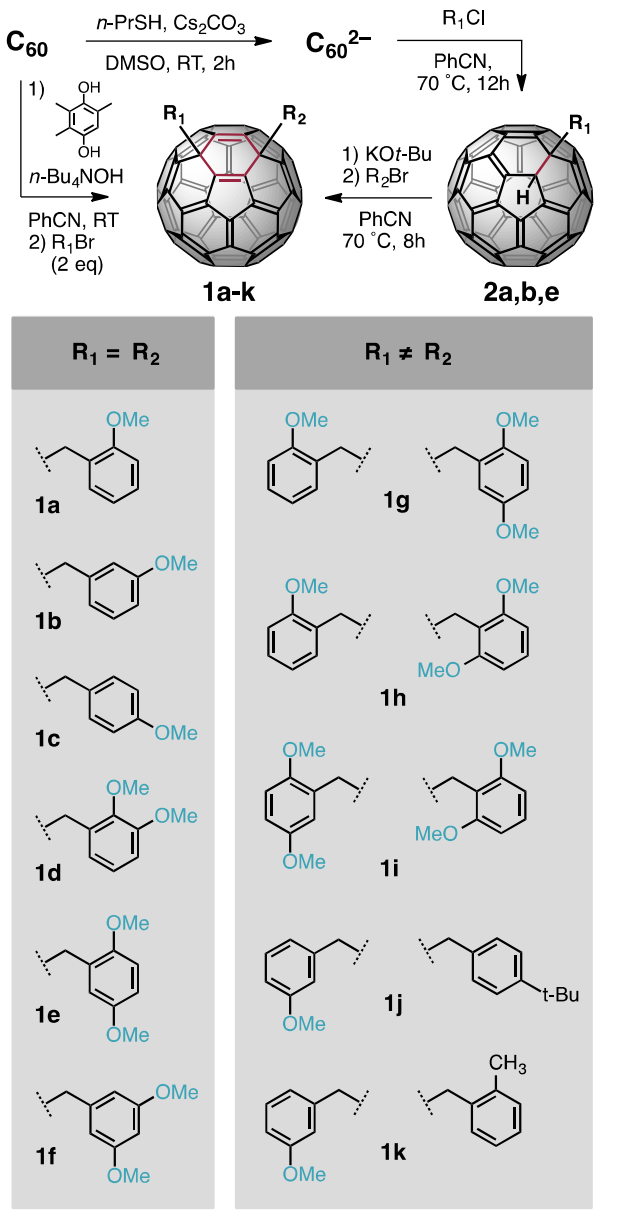

We have investigated the performance of these fullerenes in combination with both P3HT and the low-bandgap polymer PTB7.[44] The best PCE based on P3HT:1-(2',5'-dimethoxybenzyl)-4-(2",6"-dimethoxybenzyl)[60]fullerene bisadduct (**1i**) is 4.1%, which is a > 20% enhancement relative to devices made from P3HT:PCBM.

Furthermore, devices based on PTB7:**1e** show a V_{oc} of 0.83 V, a respectable *FF* (53%) and a J_{sc} (12.3 mA/cm^2) that is higher than that for devices based on PTB7:PCBM, resulting in a PCE of 5.4%. Perhaps more importantly, our results clearly

View Article Online
DOI: 10.1039/C5TA07688A

show that the precise nature and degree of substitution of the methoxy group(s), even on a single benzyl addend, greatly influences both the V_{oc} and PCE of the BHJ photovoltaic devices. Moreover, the higher conformational flexibility of the benzyl vs. an aryl substituent in these 1,4-bisadducts appears to play a significant role in obtaining high PCE values.[39,43]

Experimental

Synthesis

Our ability to synthesize the MeO-BBF bisadducts is a direct result of the ease of alkylating the C_{60} dianion.[45–50] As shown in Table 1, C_{60}^{2-} can be generated readily in dry degassed PhCN when treated with hydroquinone and base (SI).[51] By adding a large excess of a substituted benzyl bromide to a dark red solution of C_{60}^{2-}, we produced the symmetric 1,4-dibenzyl C_{60} bisadducts in relatively good yields (Table 1).

The synthesis of asymmetric 1,4-dibenzyl C_{60} bisadducts involves a stepwise alkylation procedure (SI). As shown in Table 1, C_{60} also can be reduced to C_{60}^{2-} with *n*-$PrS^{-}Cs^{+}$ generated *in situ* through the reaction of *n*-propanethiol and Cs_2CO_3 in DMSO.[52] C_{60}^{2-} reacts with substituted benzyl chlorides to provide monoadducts **2a,b** or **2e** in 50-60% yields. The lower reactivity of benzyl chlorides relative to benzyl bromides towards S_N2 is likely at the origin of the different outcomes of these two reaction conditions.[49] The subsequent benzylation of deprotonated monoadducts **2a,b** or **2e** with a benzyl bromide provides the asymmetric 1,4-bisadducts **1j–k**, which bear two different addends.

The synthesis details of each fullerene derivative and their NMR, mass-spectrometry and cyclic voltammetry characteristics can be found in the Supporting Information (SI).

Photovoltaic Device and Active Layer Fabrication Procedures

We fabricated polymer:fullerene BHJ solar cells by starting with prepatterned tin-doped indium oxide (ITO)-coated substrates (TFD Inc.) and cleaning them by successive sonication in detergent solution, deionized water, acetone and isopropanol for ~10 min each. After drying in vacuum for at least an hour, we treated the ITO substrates with an air plasma (200 mTorr, 15 min). A thin layer of poly(ethylene-dioxythiophene):poly(styrenesulfonic acid) (PEDOT:PSS) (Clevios™ P VP AI 4083) was then spin-coated onto the clean substrates in air at 5000 rpm for 20 s, and the PEDOT:PSS-covered substrate was then baked at 150 ºC for 20 min in air.

P3HT:fullerene blend solutions were prepared by dissolving solid P3HT (Rieke Metal Inc. P100) and solid fullerene derivatives in *o*-dichlorobenzene (*o*-DCB) with a weight ratio of 1:0.8. The concentration was 20 mg/mL with respect to P3HT. The solutions were stirred at 55 ºC overnight on a hot plate in a nitrogen glovebox before being cooled down to room temperature. The solutions were spun onto the PEDOT:PSS-covered substrates at 1160 rpm for 20 s. The active layers were still wet when the samples were taken off the spin-coater. Without covering or any other form of solvent annealing, the wet films became dry in the nitrogen glovebox after ~2 min. All of the films were then thermally annealed at 150 ºC for 20 min on a hot plate under an argon atmosphere. The thickness of the polymer:fullerene layers were ~160–180 nm, as measured with a Dektak 150 Stylus Surface Profiler.

PTB7:fullerene solutions were prepared by dissolving solid PTB7 (Solarmer Energy Inc.) and solid fullerene derivatives in a mixture of 95% chlorobenzene (CB)/5% 1,8-diiodooctane (DIO) v/v with a polymer:fullerene weight ratio of 1:1.5 for the fullerene bisadducts and 1:1.34 for PCBM (the change in weight ratio accounts for molecular weight differences to ensure that all polymer:fullerene blends were equimolar). The concentration was 10 mg/mL with respect to PTB7. The solutions were stirred at 55 ºC overnight prior to being spun at 1000 rpm for 60 s onto PEDOT:PSS-covered substrates. The films were then transferred to the antechamber of the glovebox and held under vacuum for ~1 hr. Pure methanol was then spun onto the films at a speed of 2500 rpm for 40 s to remove residual DIO. No further treatments were performed after this step before the deposition of the metal cathode. Cathode deposition consisted of ~10 nm of Ca evaporated at a rate of ~0.5 Å/s followed by 70 nm of Al at rates below 1 Å/s. The resulting device active areas were 7.2 mm^2.

Current density–applied voltage (*J–V*) measurements were performed in an argon atmosphere using a Keithley 2400 source meter. A xenon arc lamp and 1-sun-calibrated AM-1.5 filter were used as the excitation source.

External quantum efficiency (EQE) measurements were taken using a home-built set-up that has been detailed in previous publications by our group.[53]

Films for non-device measurements were prepared using identical procedures to those described above but without deposition of a top electrode.

Structural and Optical Characterization

UV-Visible absorption spectra were collected using a Perkin-Elmer Lambda 25 UV/Vis Spectrophotometer.

The 2-D grazing incidence wide angle X-ray scattering (GIWAXS) experiments were performed at the Stanford Synchrotron Radiation Lightsource on beamline 11-3 using a wavelength of 0.9742 Å. Figure 3c in the next section was obtained by radially-integrating the full 2-D diffractograms. Each data curve in Fig. 3c is the average of at least three different samples prepared using the same conditions. The 2-D images were collected on a plate with the detector 400 mm away from the center of the measured sample. The beam spot had a width of ~150 µm. A helium chamber was used to reduce the noise. The software package WxDiff was used to analyze the GIWAXS data.

Results and discussion

Material properties

Fullerene derivatives **1a–k** all have good solubility in common organic solvents for solar cell fabrication, such as $CHCl_3$, CS_2, CB and *o*-DCB. The products were characterized by mass spectrometry, ^{1}H-NMR and ^{13}C-NMR (SI) spectroscopy. The ^{1}H-NMR spectra show that the peaks of methylene groups are

View Article Online
DOI: 10.1039/C5TA07688A

split into AB quartets for the symmetrical 1,4-bisadducts **1a–f**, and mostly split into four doublets for unsymmetrical **1g–k** (see SI), which implies the 1,4-addition pattern. Single crystals of **1c** and **1e** were obtained through slow diffusion of EtOH into a CS_2 solution, providing the X-ray structures shown in Fig. 1. Their structures show a number of short intermolecular C–C contact distances between fullerene carbons, as shown in Fig. 1b,e; these short packing distances should favor electron mobility through increased intermolecular orbital interactions. The shortest contacts are 3.301 Å and 3.028 Å for **1c** and **1e**, respectively. Despite the different short-contact distances, both structures have a similar 2-D layered structure and an interpenetrating network of methoxylated benzyl groups. The opposite side of the interpenetrated network of methoxylated benzyl groups is a fullerene bilayer displaying a number of fullerene-fullerene close-contacts (Fig. 1c,f).

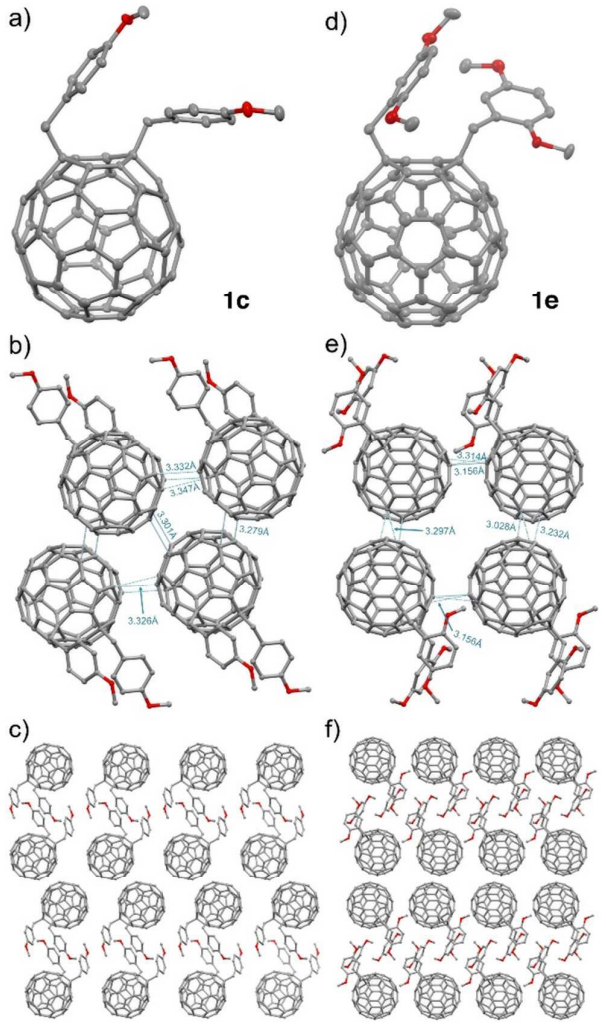

Fig. 1 a,d) ORTEP representations of the single crystal structures for 1,4-bisadducts **1c** and **1e**, respectively. b,e) Packing modes and intermolecular C–C contacts shorter than van der Waals distances (≤ 0.05 Å) for **1c** and **1e**, respectively. c,f) Packing structures for **1c** down the crystallographic *a*-axis, and **1e** down the crystallographic *b*-axis, respectively. Both are 2-D layered structures. Hydrogens and CS_2 cocrystallization solvent molecules are omitted for clarity.

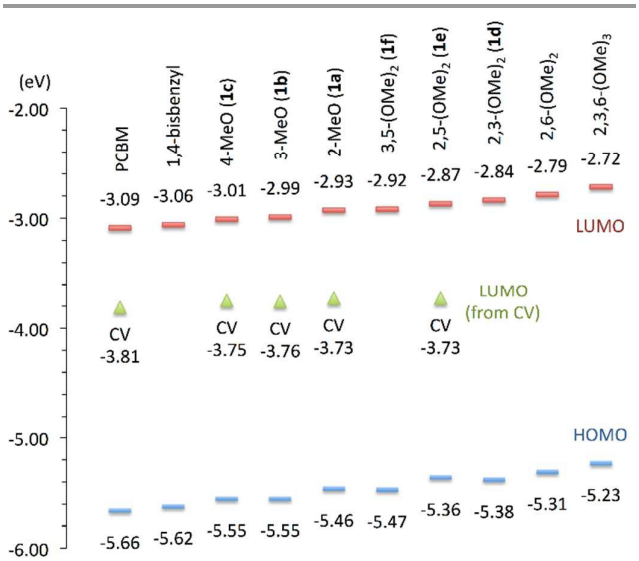

Fig. 2 DFT (B3LYP/6-31G(d)) calculated HOMO (red dash) and LUMO (blue dash) energies and selected LUMOs from experimental CV data (green triangle) for PCBM and symmetrically substituted 1,4-bisbenzyl [60]fullerene adducts (i.e. R_1=R_2 in Table 1) where the compound legend after PCBM and 1,4-bisbenzyl indicates the relative position(s) of methoxy group(s) on the benzyl substituents.

The green triangles in Fig. 2 show the electrochemical properties of several selected MeO-BBFs. These cyclic voltammetry (CV) measurements show that the LUMO levels of our MeO-BBFs are higher than that of PCBM by ~0.05–0.09 eV, depending on the position of the methoxy substituent. Methoxy substitution at the 2-position results in a slightly higher LUMO level than substitution at the 3- or 4-positions.

DFT calculations (B3LYP/6-31G(d)) of the HOMO and LUMO levels of MeO-BBFs **1a–f** also show the same trend in increasing HOMO and LUMO energies as the relative placement of the methoxy group changes from the 2- to the 3- and 4-positions (Fig. 2), although the absolute values do not agree with experiment, as expected for a calculation of this type. Furthermore, increasing the number of methoxy substituents also steadily raises both the HOMO and LUMO energies. This effect of substitution can be explained by the Wheeler-Houk model:[54–56] since there can be only negligible overlap between the π-systems of the benzyl substituents and the fullerene, the interaction between them is primarily electrostatic. Thus, proximal oxygen lone pairs can increase electron density on the fullerene π-system. A methoxy group at the 2-position has its lone pairs closest to the fullerene π-system, while methoxy groups at the 3- or 4-positions show less interaction as the average distance increases. Similarly, increasing the number of methoxy groups from one (**1a–c**) to two (**1d–f** or 1,4-bis[2,6-dimethoxybenzyl]) or three (1,4-bis[2,3,6-trimethoxybenzyl]) results in easier ionization and makes reduction become more difficult (Fig. 2).

Photovoltaic device performance and structural characterization

To examine the performance of the MeO-BBF **1a–k** in BHJ solar cells, we first blended our new fullerene derivatives with

View Article Online
DOI: 10.1039/C5TA07688A
Journal of Materials Chemistry A ARTICLE

P3HT and fabricated photovoltaic devices with a structure glass/ITO/PEDOT:PSS (30 nm)/1:0.8 polymer:fullerene (~160-180 nm)/Ca(10 nm)/Al (70 nm). All of the performance comparisons and conclusions we draw are based on the study of devices with composition- and thickness-matched active layers.

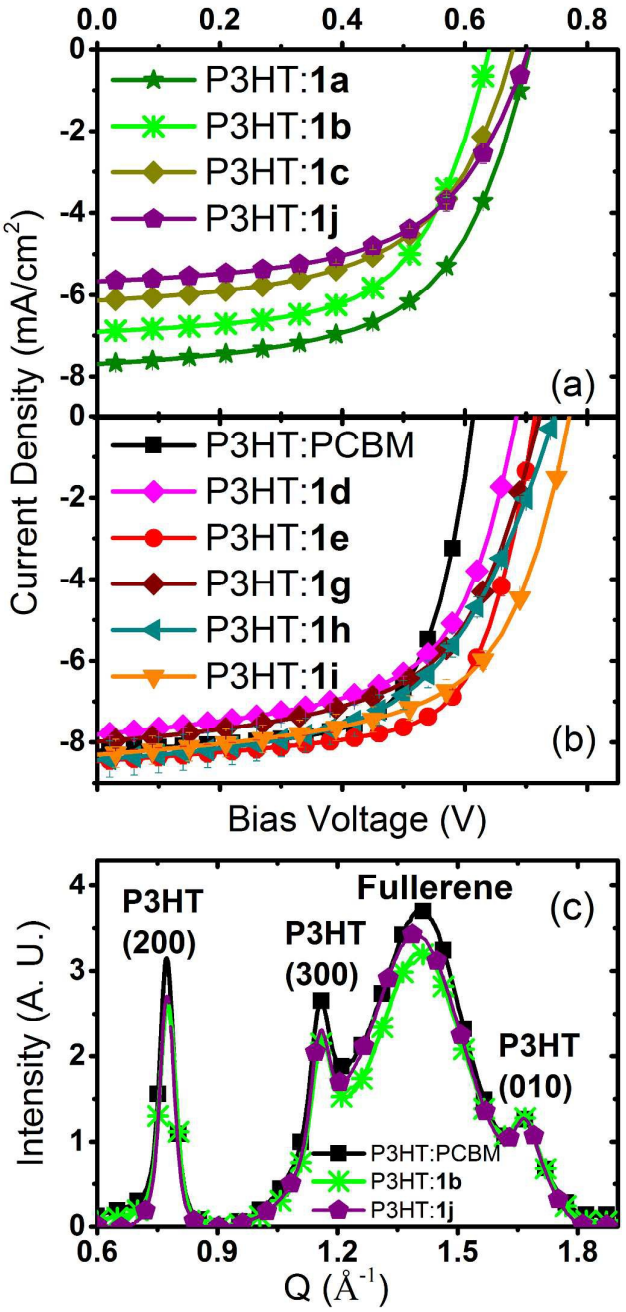

Fig. 3 (a) and (b): Current density versus applied bias for photovoltaic devices based on P3HT:MeO-BBFs where each of the benzyl rings in the MeO-BBFs are substituted with one side group (a) and two methoxy groups (b). The *J-V* curve of a standard P3HT:PCBM-based control device is plotted in (b) as the black curve/squares. The error bars show 1 standard deviation for measurements over at least 6 independent devices. (c): Example of radially-integrated 2-D GIWAXS intensities for three P3HT:fullerene active layers processed on silicon substrates.

All active layers were thermally annealed at 150 °C for 20 min prior to deposition of the cathode, and *J–V* curves were measured under AM 1.5G illumination.

Figure 3a and Table 2 summarize the performance of P3HT:MeO-BBF-based devices where the benzyl rings connected to the fullerene ball have substituents with a single side group (**1a–1c, 1j, 1k**). We find that non-methoxy substituents on even one of the benzyl rings resulted in either lower *FF*s (P3HT:**1k**) or lower J_{sc}'s (P3HT:**1j**) than benzyl groups with methoxy substitution; the PCE's for devices based on non-methoxylated 1,4-bisadducts were in the relatively low range of 2.2 to 2.4%. In contrast, methoxy substitution led to higher-performing devices (PCE's ranging from 2.3 to 3.1% for P3HT:**1a**) depending on the exact position at which the methoxy groups were substituted.

Table 2. Summary of Photovoltaic Device Parameters

BHJ	V_{oc} (mV)	J_{sc} (mA/cm^2)	*FF* (%)	*PCE* (%)
P3HT:PCBM	613 ± 2	8.2 ± 0.2	66.6 ± 0.4	3.4 ± 0.1
P3HT:**1a**	716 ± 5	7.6 ± 0.3	57.6 ± 1.1	3.1 ± 0.1
P3HT:**1b**	640 ± 4	6.9 ± 0.2	59.4 ± 0.6	2.6 ± 0.1
P3HT:**1c**	679 ± 2	6.1 ± 0.2	55.4 ± 1.6	2.3 ± 0.1
P3HT:**1d**	680 ± 1	7.8 ± 0.1	59.7 ± 1.1	3.2 ± 0.1
P3HT:**1e**	715 ± 1	8.5 ± 0.2	66.3 ± 0.7	3.9 ± 0.1
P3HT:**1f**	588 ± 5	6.0 ± 0.1	55.4 ± 1.3	2.0 ± 0.1
P3HT:**1g**	720 ± 1	8.0 ± 0.2	57.5 ± 0.1	3.3 ± 0.1
P3HT:**1h**	740 ± 1	8.4 ± 0.5	55.0 ± 0.1	3.4 ± 0.2
P3HT:**1i**	771 ± 2	8.3 ± 0.3	60.1 ± 0.8	3.9 ± 0.2
P3HT:**1j**	704 ± 1	5.7 ± 0.3	56.1 ± 1.5	2.2 ± 0.1
P3HT:**1k**	667 ± 4	7.2 ± 0.1	49.2 ± 1.1	2.4 ± 0.1
PTB7:PCBM	760 ± 1	12.1 ± 0.2	64.4 ± 0.1	5.9 ± 0.3
PTB7:**1e**	825 ± 9	12.3 ± 0.2	53.3 ± 0.1	5.4 ± 0.1

To understand why such subtle variations in the substitution pattern of our 1,4-bisadducts led to such widely varying device performance, we studied the morphology of the solar cell active layers using GIWAXS. The experiments were performed at the Stanford Synchrotron Radiation Light Source on beamline 11−3 with a wavelength of 0.9742 Å. For these experiments, we focused on three selected polymer:fullerene systems: P3HT:PCBM, P3HT:**1b** and P3HT:**1j** (Fig. 3c).

In pure films, P3HT orients with the chains edge-on to the substrate,[57–60] and based on the relative in-plane and out-of plane scattering intensities, we see that this preferred chain orientation is maintained upon addition of either MeO-BBF or PCBM (see SI). However, both the characteristic fullerene diffraction observed at ~1.4 Å^{-1} and the crystallinity of the P3HT (as measured by the intensity of the (200) peak) are smaller when **1b** or **1j** are used in the active layer compared to when PCBM is used. Lower crystallinity materials should have a poorer carrier mobility, which could explain the lower J_{sc} and *FF* of the photovoltaic devices based on these active layers.[60] Another notable difference is that for P3HT:**1j**, the fullerene peak is shifted towards lower *Q*, which corresponds to an increased spacing between fullerenes. Fullerene **1j** contains a bulky *t*-butyl group substituted on one benzyl ring, which likely hinders close packing of the fullerene molecules. Consequently,

View Article Online
DOI: 10.1039/C5TA07688A

this increase in inter-fullerene spacing leads to a decreased electronic coupling between fullerenes and therefore to a decrease in carrier mobility.[27] This is also consistent with **1j** having the lowest J_{sc} among all the MEO-BBFs.

Figure 3a and Table 2 also show that when the methoxy group is at the 2-position of the benzyl group (**1a**), the corresponding device has a greater PCE (3.1%) compared to the 3-position (2.6%, **1b**), which in turn is greater than with the 4-position (2.3%, **1c**). The changes in V_{oc} (Table 2) of these three devices track the changes in experimental (CV) and DFT-calculated LUMO levels of MeO-BBFs **1a–f** (Fig. 2).

Although electrostatic interactions can explain the changes in V_{oc}, the variation in the J_{sc} of the devices cannot be easily explained by the electrochemical or computational results. There are two potential reasons for the sensitivity of the photocurrent to the substitution position. First, the position of the methoxy group can affect the fullerene-to-fullerene contact distance and thus the electronic coupling and local carrier mobility. Second, the way the fullerene interacts with the polymer could be altered by the structure of the benzyl side chain, which would alter the resultant BHJ morphology. Finally, the propensity of the fullerene to crystallize could alter the polymer/fullerene phase separation, again changing the overall BHJ morphology.

To investigate this, we measured the diode ideality factor, n_{ideal}, for each of the MeO-BBF-based devices by fitting their dark *J–V* curves (Table 3); n_{ideal} provides an indicator of the charge carrier recombination mechanism.[61,62] Table 3 in the SI shows that devices with P3HT:**1a** have the most ideal (i.e., closest to bimolecular rather than trap-dominated) recombination among fullerene derivatives **1a–c**, suggesting that the variations in J_{sc} predominantly reflect changes in BHJ morphology.

Table 3. Summary of Photovoltaic Device Parameters

BHJ	n_{ideal}	R_{seires} (Ω-cm^2)	R_{shunt} ($\times 10^5$ Ω-cm^2)
P3HT:PCBM	1.34 ± 0.03	3.2 ± 0.1	2.0 ± 0.1
P3HT:**1a**	1.40 ± 0.02	4.4 ± 0.4	29 ± 7
P3HT:**1b**	1.80 ± 0.15	3.5 ± 0.2	1.2 ± 0.6
P3HT:**1c**	1.44 ± 0.03	6.0 ± 0.6	14 ± 0.8
P3HT:**1d**	1.39 ± 0.03	4.0 ± 0.3	8.0 ± 0.2
P3HT:**1e**	1.31 ± 0.01	3.3 ± 0.1	20 ± 6
P3HT:**1f**	1.63 ± 0.04	3.8 ± 1.5	3.5 ± 0.7
P3HT:**1g**	1.27 ± 0.01	4.2 ± 0.8	37 ± 3
P3HT:**1h**	1.41 ± 0.02	3.2 ± 0.1	7.5 ± 0.4
P3HT:**1i**	1.28 ± 0.03	3.3 ± 0.1	43 ± 17
P3HT:**1j**	1.44 ± 0.04	6.0 ± 0.9	16 ± 4
P3HT:**1k**	1.51 ± 0.02	3.8 ± 0.6	42 ± 12
PTB7:PCBM	1.37 ± 0.01	1.5 ± 0.1	0.1 ± 0.01
PTB7:**1e**	1.37 ± 0.01	3.7 ± 0.4	0.7 ± 0.2

After establishing that alkyl group substitution on the benzyl ring was inferior to methoxy group substitution for solar cell performance, we next turned to study the effects of the number and position of the methoxy substituents. To this end, we synthesized fullerene derivatives **1d–1i** (Table 1), and fabricated photovoltaic devices from those derivatives. The performance parameters are again summarized in Table 2. Examples of the *J–V* curves for these devices under AM1.5G illumination are plotted in Fig. 3b.

The most striking result of Fig. 3b and Table 2 is that 1,4-bisadduct fullerenes with bismethoxy-substituted benzyl rings lead to improved solar cell efficiency; in fact, most of the PCEs reach or surpass those of P3HT:PCBM. Both P3HT:**1e** and P3HT:**1i** show a ~20% enhancement in PCE compared to P3HT:PCBM (black squares in Fig. 3), and P3HT:**1d**, P3HT:**1g** and P3HT:**1h** all have comparable PCEs to P3HT:PCBM devices. P3HT:**1f** is clearly an exception, having the lowest PCE of the group, and we are currently investigating the morphology of this active layer to understand why.

Compared to the monomethoxy MeO-BBFs **1a–1c**, devices fabricated using **1d–1i** (except for **1f**) show both higher J_{sc} and V_{oc}. We measured n_{ideal} values for these devices (Table 3), and found the general trend that devices based on **1d–1i** have more ideal charge carrier recombination than those based on **1a–1c**. This indicates that the nanoscale BHJ morphology is improved by the addition of the second methoxy group on the benzyl rings of the MeO-BBFs. This morphology improvement also likely contributes to the increase in both J_{sc} and V_{oc}.

Figure 3b and Table 2 also reinforce the observation that the position of the methoxy group(s) has a significant effect on device performance. The dependence of V_{oc} on methoxy position can be summarized as follows: placing methoxy groups at the 2- or 2,6-positions increases V_{oc}, whereas placing methoxy groups at the 3- or 5- positions lowers the V_{oc}. In fact, fullerenes with two methoxy groups at the 3- (or 5-) position, such as **1d** and **1e**, show lower V_{oc} than those with fewer, such as **1g**, **1h** and **1i**. When both methoxy groups are at the 3- and 5- positions, as with fullerene **1f**, the resultant device shows the lowest V_{oc}. With this trend in mind, we then synthesized the MeO-BBF derivative with methoxy groups at the 2,6-positions of each benzyl ring, which in principle should be the best-performing derivative. Unfortunately, this compound was not soluble enough in the solvents needed for device fabrication, so we could not test it in an organic photovoltaic device.

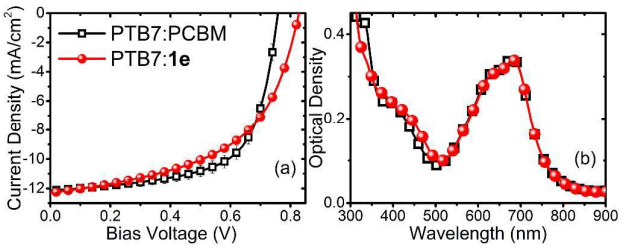

Fig. 4 a) Current density versus applied bias for photovoltaic devices based on PTB7:PCBM (open black square) and PTB7:**1e** (red circle). The error bars show 1 standard deviation for measurements over at least 6 independent devices. b) UV-visible absorption spectra for the same active layers used in (a).

As mentioned in the introduction, the most successful high-LUMO fullerenes studied to date (e.g., ICBA and its C_{70} analog) show poor compatibility with modern low bandgap push-pull polymers. To see if we could break this trend with our MeO-BBF derivatives, we investigated the compatibility of one of our best derivatives (**1e**) with the high-performance low-

View Article Online
DOI: 10.1039/C5TA07688A
Journal of Materials Chemistry A ARTICLE

bandgap polymer PTB7 (Fig. 4). We employed the same device structure, with the active layer consisting of PTB7 and **1e** at a polymer:fullerene weight ratio of 1:1.5 with a thickness of ~90 nm. These active layers were used as-cast, without thermal annealing prior to cathode deposition. For comparison, we also fabricated PTB7:PCBM control devices, taking care to keep the two sets of devices thickness- and composition-matched, as shown by UV-Vis absorption (Fig. 4b).

Figure 4a and the bottom portion of Table 2 summarize the device performance results. Clearly, fullerene **1e**, which showed the best performance when blended with P3HT, also demonstrates excellent compatibility with PTB7. PTB7:**1e** devices show a higher V_{oc} and a similarly high J_{sc} as PTB7:PCBM devices. The overall device efficiency of PTB7:**1e** is slightly lower than PTB7:PCBM, however, due to a slightly lower *FF* that may be due to less efficient crystallization of derivative **1e** compared to PCBM, changing the resultant BHJ morphology.

Conclusions

In summary, we have synthesized a series of methoxylated 1,4-[60]fullerene bisadducts, **1a–k**, which have higher LUMO levels than PCBM. We evaluated their performance in BHJ solar cells and compared the resulting BHJ morphologies to those of the workhorse fullerene PCBM. Our best fullerene derivatives show more than 20% enhancement in device efficiency when combined with P3HT, largely due to the improved V_{oc} resulting from the higher LUMO of the 1,4-bis-substituted fullerenes. We found that adding methoxy groups to the benzyl rings increases the device performance and that the number and position of these groups has a dramatic effect on the solar cell efficiency due to morphological changes. Unlike previously-studied fullerene bisadducts, which are outperformed by PCBM when combined into BHJs with low bandgap polymers, our 1,4-bisadduct **1e** demonstrated good compatibility with one of the best performing red polymers, PTB7. We are currently working on a deeper understanding of both the device physics and active-layer morphologies for these fullerene derivatives in polymer solar cells to help guide further synthesis and increase device performance. We believe that 1,4-bisbenzyl fullerene bisadducts in general and future C_{70} analogs of these molecules are promising candidates for replacing PCBM to improve the performance of conjugated polymer-based solar cells.

Acknowledgements

We thank Prof. Kendall N. Houk for his insightful suggestions on the DFT calculations. This work was supported by the Center for Molecularly Engineered Energy Materials (MEEM), an Energy Frontier Research Center (EFRC) funded by the U.S. Department of Energy (DOE), Office of Science, Office of Basic Energy Sciences (BES) under Contract Number DE-AC06-76RLO-1830 (device studies, X-ray diffraction, manuscript preparation). Additional support was provided by the National Science Foundation under Grants CHE-1112569 and CBET- 1510353 (optical, device studies, and fullerene synthesis). Portions of this research were carried out at the Stanford Synchrotron Radiation Lightsource, a Directorate of SLAC National Accelerator Laboratory and an Office of Science User Facility operated for the U.S. Department of Energy Office of Science by Stanford University.

References

1 C. Deibel and V. Dyakonov, *Rep. Prog. Phys*, 2010, **73**, 096401.
2 M. Jørgensen, J. E. Carlé, R. R. Søndergaard, M. Lauritzen, N. A. Dagnæs-Hansen, S. L. Byskov, T. R. Andersen, T. T. Larsen-Olsen, A. P. L. Böttiger, B. Andreasen, L. Fu, L. Zuo, Y. Liu, E. Bundgaard, X. Zhan, H. Chen and F. C. Krebs, *Sol. Energy Mater. Sol. Cells*, 2013, **119**, 84–93.
3 F. C. Krebs, N. Espinosa, M. Hösel, R. R. Søndergaard and M. Jørgensen, *Adv. Mater.*, 2014, **26**, 29–39.
4 R. R. Søndergaard, M. Hösel and F. C. Krebs, *J. Polym. Sci. Part B Polym. Phys.*, 2013, **51**, 16–34.
5 M. C. Scharber and N. S. Sariciftci, *Prog. Polym. Sci.*, 2013, **38**, 1929–1940.
6 G. Yu, J. Gao, J. C. Hummelen, F. Wudl and A. J. Heeger, *Science (80-.).*, 1995, **270**, 1789–1791.
7 A. J. Heeger, *Adv. Mater.*, 2014, **26**, 10–27.
8 C.-Z. Li, H.-L. Yip and A. K.-Y. Jen, *J. Mater. Chem.*, 2012, **22**, 4161.
9 Y. Liu, J. Zhao, Z. Li, C. Mu, W. Ma, H. Hu, K. Jiang, H. Lin, H. Ade and H. Yan, *Nat. Commun.*, 2014, **5**, 5293.
10 H. Zhou, L. Yang and W. You, *Macromolecules*, 2012.
11 I. Etxebarria, J. Ajuria and R. Pacios, *Org. Electron.*, 2015, **19**, 34–60.
12 Z. He, C. Zhong, S. Su, M. Xu, H. Wu and Y. Cao, *Nat. Photonics*, 2012, **6**, 591–595.
13 J. C. Hummelen, B. W. Knight, F. Lepeq, F. Wudl, J. Yao and C. L. Wilkins, *J. Org. Chem.*, 1995, **60**, 532–538.
14 M. M. Wienk, J. M. Kroon, W. J. H. Verhees, J. Knol, J. C. Hummelen, P. a van Hal and R. A. J. Janssen, *Angew. Chem. Int. Ed. Engl.*, 2003, **42**, 3371–5.
15 Y. He, H. Chen, J. Hou and Y. Li, *J. Am. Chem. Soc.*, 2010, **132**, 1377–1382.
16 Y. He and Y. Li, *Phys. Chem. Chem. Phys.*, 2011, **13**, 1970–83.
17 X. Meng, Q. Xu, W. Zhang, Z. Tan, Y. Li, Z. Zhang, L. Jiang, C. Shu and C. Wang, *ACS Appl. Mater. Interfaces*, 2012, **4**, 5966–5973.
18 C. Zhang, S. Chen, Z. Xiao, Q. Zuo and L. Ding, *Org. Lett.*, 2012, **14**, 1508–1511.
19 B. Kim, J. Lee, J. H. Seo, F. Wudl, S. H. Park and C. Yang, *J. Mater. Chem.*, 2012, **22**, 22958.
20 Y. He, M. Shao, K. Xiao, S. C. Smith and K. Hong, *Sol. Energy Mater. Sol. Cells*, 2013, **118**, 171–178.
21 S. Chen, G. Ye, Z. Xiao and L. Ding, *J. Mater. Chem. A*, 2013, **1**, 5562–5566.
22 D. He, C. Zuo, S. Chen, Z. Xiao and L. Ding, *Phys. Chem. Chem. Phys.*, 2014, **16**, 7205–7208.
23 D. He, X. Du, Z. Xiao and L. Ding, *Org. Lett.*, 2014, **16**, 612–615.
24 G. Ye, S. Chen, Z. Xiao, Q. Zuo, Q. Wei and L. Ding, *J. Mater. Chem.*, 2012, **22**, 22374–22377.
25 J.-H. Huang, Y.-S. Hsiao, E. Richard, C.-C. Chen, P. Chen, G. Li, C.-W. Chu and Y. Yang, *Appl. Phys. Lett.*, 2013, **103**, 043304.

View Article Online
DOI: 10.1039/C5TA07688A

26 M. A. Faist, S. Shoaee, S. Tuladhar, G. F. A. Dibb, S. Foster, W. Gong, T. Kirchartz, D. D. C. Bradley, J. R. Durrant and J. Nelson, *Adv. Energy Mater.*, 2013, **3**, 744–752.
27 J. C. Aguirre, C. Arntsen, S. Hernandez, R. Huber, A. M. Nardes, M. Halim, D. Kilbride, N. Kopidakis, S. H. Tolbert, B. J. Schwartz and N. Daniel, *Adv. Funct. Mater.*, 2013, **24**, 784–792.
28 M. Lenes, G.-J. A. H. Wetzelaer, F. B. Kooistra, S. C. Veenstra, J. C. Hummelen and P. W. M. Blom, *Adv. Mater.*, 2008, **20**, 2116–2119.
29 Y. He, G. Zhao, B. Peng and Y. Li, *Adv. Funct. Mater.*, 2010, **20**, 3383–3389.
30 X. Meng, G. Zhao, Q. Xu, Z. Tan, Z. Zhang, L. Jiang, C. Shu, C. Wang and Y. Li, *Adv. Funct. Mater.*, 2014, **24**, 158–163.
31 Y.-J. Cheng, M.-H. Liao, C.-Y. Chang, W.-S. Kao, C.-E. Wu and C.-S. Hsu, *Chem. Mater.*, 2011, **23**, 4056–4062.
32 N. C. Miller, S. Sweetnam, E. T. Hoke, R. Gysel, C. E. Miller, J. A. Bartelt, X. Xie, M. F. Toney and M. D. McGehee, *Nano Lett.*, 2012, **12**, 1566–70.
33 D. Di Nuzzo, G.-J. A. H. Wetzelaer, R. K. M. Bouwer, V. S. Gevaerts, S. C. J. Meskers, J. C. Hummelen, P. W. M. Blom and R. A. J. Janssen, *Adv. Energy Mater.*, 2013, **3**, 85–94.
34 S. Shoaee, S. Subramaniyan, H. Xin, C. Keiderling, P. S. Tuladhar, F. Jamieson, S. A. Jenekhe and J. R. Durrant, *Adv. Funct. Mater.*, 2013, **23**, 3286–3298.
35 A. A. Bakulin, A. Rao, V. G. Pavelyev, P. H. M. van Loosdrecht, M. S. Pshenichnikov, D. Niedzialek, J. Cornil, D. Beljonne and R. H. Friend, *Science*, 2012, **335**, 1340–4.
36 C. J. Brabec, C. Winder, N. S. Sariciftci, J. C. Hummelen, A. Dhanabalan, P. A. van Hal and R. A. J. Janssen, *Adv. Funct. Mater.*, 2002, **12**, 709–712.
37 W. Li, W. S. C. Roelofs, M. M. Wienk and R. A. J. Janssen, *J. Am. Chem. Soc.*, 2012, **134**, 13787–95.
38 A. B. Sieval, N. D. Treat, D. Rozema, J. C. Hummelen and N. Stingelin, *Chem. Commun.*, 2015, **51**, 8126–8129.
39 Y. Matsuo, H. Oyama, I. Soga, T. Okamoto, H. Tanaka, A. Saeki, S. Seki and E. Nakamura, *Chem. Asian J.*, 2013, **8**, 121–128.
40 Y. Matsuo, A. Iwashita, Y. Abe, C.-Z. Li, K. Matsuo, M. Hashiguchi and E. Nakamura, *J. Am. Chem. Soc.*, 2008, **130**, 15429–15436.
41 Y. Matsuo, Y. Sato, T. Niinomi, I. Soga, H. Tanaka and E. Nakamura, *J. Am. Chem. Soc.*, 2009, **131**, 16048–16050.
42 H. Tanaka, Y. Abe, Y. Matsuo, J. Kawai, I. Soga, Y. Sato and E. Nakamura, *Adv. Mater.*, 2012, **24**, 3521–3525.
43 A. Varotto, N. D. Treat, J. Jo, C. G. Shuttle, N. A. Batara, F. G. Brunetti, J. H. Seo, M. L. Chabinyc, C. J. Hawker, A. J. Heeger and F. Wudl, *Angew. Chem. Int. Ed.*, 2011, **50**, 5166–5169.
44 Y. Liang, Z. Xu, J. Xia, S.-T. Tsai, Y. Wu, G. Li, C. Ray and L. Yu, *Adv. Mater.*, 2010, **22**, 1–4.
45 R. Subramanian, K. M. Kadish, M. N. Vijayashree, X. Gao, M. T. Jones, M. D. Miller, K. L. Krause, T. Suenobu and S. Fukuzumi, *J. Phys. Chem.*, 1996, **100**, 16327–16335.
46 E. Allard, L. Rivitre, J. Delaunay, D. Dubois and J. Cousseau, *Tetrahedron Lett.*, 1999, **40**, 7223–7226.
47 F. Cheng, Y. Murata and K. Komatsu, *Org. Lett.*, 2002, **4**, 2541–2544.
48 E. Allard, J. Delaunay and J. Cousseau, *Org. Lett.*, 2003, **5**, 2239–2242.
49 E. Allard, F. Cheng, S. Chopin, J. Delaunay, D. Rondeau and J. Cousseau, *New J. Chem.*, 2003, **27**, 188–192.
50 J. Cousseau, E. Allard and S. Chopin, *Comptes Rendus Chim.*, 2006, **9**, 1051–1057.
51 M. Toganoh, K. Suzuki, R. Udagawa, A. Hirai, M. Sawamura and E. Nakamura, *Org. Biomol. Chemsitry*, 2003, **1**, 2604–2611.
52 R. Subramanian, P. Boulas, M. N. Vijayashree, F. D'Souza, M. T. Jones and K. M. Kadish, *J. Chem. Soc. Chem. Commun.*, 1994, 1847.
53 S. A. Hawks, J. C. Aguirre, L. T. Schelhas, R. J. Thompson, R. C. Huber, A. S. Ferreira, G. Zhang, A. A. Herzing, S. H. Tolbert and B. J. Schwartz, *J. Phys. Chem. C*, 2014, **118**, 17413–17425.
54 S. E. Wheeler and K. N. Houk, *J. Am. Chem. Soc.*, 2008, **130**, 10854–10855.
55 S. E. Wheeler, *J. Am. Chem. Soc.*, 2011, **133**, 10262–10274.
56 For a different explanation of the effect of substitution on PCBM derivatives, see: F. B. Kooistra, J. Knol, F. Kastenberg, L. M. Popescu, W. J. H. Verhees, J. M. Kroon and J. C. Hummelen, *Org. Lett.*, 2007, **9**, 551–554.
57 H. Sirringhaus, P. J. Brown, R. H. Friend, M. M. Nielsen, K. Bechgaard, B. M. W. Langeveld-Voss, A. J. H. Spiering, R. A. J. Janssen, E. W. Meijer, P. Herwig and D. M. de Leeuw, *Nature*, 1999, **401**, 685–688.
58 M. Sanyal, B. Schmidt-Hansberg, M. F. G. Klein, A. Colsmann, C. Munuera, A. Vorobiev, U. Lemmer, W. Schabel, H. Dosch and E. Barrena, *Adv. Energy Mater.*, 2011, **1**, 363–367.
59 Y. Kim, S. Cook, S. M. Tuladhar, S. A. Choulis, J. Nelson, J. R. Durrant, D. D. C. Bradley, M. Giles, I. McCulloch, C.-S. Ha and M. Ree, *Nat. Mater.*, 2006, **5**, 197–203.
60 G. Zhang, R. C. Huber, A. S. Ferreira, S. D. Boyd, C. K. Luscombe, S. H. Tolbert and B. J. Schwartz, *J. Phys. Chem. C*, 2014, **118**, 18424–18435.
61 G. A. H. Wetzelaer, M. Kuik, M. Lenes and P. W. M. Blom, *Appl. Phys. Lett.*, 2011, **99**, 153506.
62 R. A. Street, A. Krakaris and S. R. Cowan, *Adv. Funct. Mater.*, 2012, **22**, 4608–4619.